

Bomb Damage Assessment Using a Dispensed Sensor Projectile

GEOFFREY FROST
MARK COSTELLO
Oregon State University

The problem of obtaining images of a target site after munition impact is approached by releasing a small projectile equipped with a camera from a dropped munition. A ballute is deployed from the sensor projectile shortly after release from the munition. This type of system is capable of viewing munition impact and subsequent target effects over a wide variety of conditions and offers the possibility of real-time battle damage assessment (BDA). However, fundamental limits exist on the duration that the camera is able to view the target after impact for a particular required separation distance between the sensor projectile and the target at impact and the field of regard (FOR) of the camera. Munition release altitude and velocity significantly affect these fundamental limits. Optimal performance is attained under high altitude and low speed munition drop conditions. Basic characteristics of the camera projectile also significantly influence system performance. Maximum target view time is attained with a low weight high drag configuration. To reduce the maximum acceleration experienced by the sensor projectile, a small delay time between the release of the small sensor projectile from the munition and inflation of ballute is required.

Manuscript received March 21, 2001; revised July 19, 2002; released for publication April 28, 2003.

IEEE Log No. T-AES/39/3/818483.

Refereeing of this contribution was handled by T. F. Roome.

Authors' address: Dept. of Mechanical Engineering,
Oregon State University, Corvallis, OR 97331, E-mail:
(COSTELLO@eng.ORST.edu).

0018-9251/03/\$17.00 © 2003 IEEE

NOMENCLATURE

x, y, z	Components of position vector of center of mass of composite body in an inertial reference frame
ϕ, θ, ψ	Euler roll, pitch and yaw angles of projectile
u, v, w	Components of velocity vector of mass center of composite body in body reference frame
p, q, r	Components of angular velocity vector of projectile in body reference frame
X, Y, Z	Total applied force components in aft body reference frame
L, M, N	Total applied moments about body mass center expressed in aft body reference frame
V	Magnitude of velocity vector of mass center of projectile
V_{MW}	Mean atmospheric wind expressed in inertial reference frame
ρ	Air density
D	Projectile reference diameter
F_S	Separation force between lead and follower projectiles
n_x, n_y, n_z	Direction cosines of separation force between lead and follower projectiles
C_{X0}	Zero yaw axial force aerodynamic coefficient
C_{X2}	Yaw axial force aerodynamic coefficient
C_{NA}	Normal force aerodynamic coefficient
C_{DD}	Fin cant roll moment aerodynamic coefficient
C_{LP}	Roll damping aerodynamic coefficient
C_{MQ}	Pitch damping aerodynamic coefficient
SL_{CG}	Stationline of follower projectile mass center measured from base along \bar{i} body axis
BL_{CG}	Buttline of follower projectile mass center measured from axis of symmetry along \bar{j} . Body axis
WL_{CG}	Waterline of follower projectile mass center point measured from axis of symmetry along \bar{k} . Body axis
SL_C	Stationline of camera focal point measured from base of follower projectile along \bar{i} body axis
BL_C	Buttline of camera focal point measured from axis of symmetry of follower projectile along \bar{j} . Body axis
WL_C	Waterline of camera focal point measured from axis of symmetry of follower projectile along \bar{k} . Body axis.

INTRODUCTION

The modern battlefield is a complex array of friendly assets interacting with enemy targets. In the case of air warfare, the commander has a diverse set of delivery platforms and weapons available to engage a particular target. Timely information regarding the status of enemy targets is critical to effective battlefield management. Battle damage assessment (BDA) is accomplished by recording images of a target area after an engagement and subsequently analyzing the images to determine the status of a target. Currently, images are recorded by satellite and aircraft reconnaissance, cameras mounted on a parent aircraft, and unmanned aerial vehicles. Images recorded by satellites and high altitude aircraft are hampered by poor weather conditions around a target and useful target images may take days to acquire in certain geographic areas. Image recording systems onboard aircraft assets include target designation video systems for guided bombs or gun cameras. Future fire and forget weapons released from aircraft at altitude will not be able to provide direct BDA information since these delivery platforms will depart the target area before munition impact. Unmanned aerial vehicles operating on the battlefield provide targeting information before an engagement as well as BDA after an engagement. The sheer volume of munitions dropped on different targets is problematic for real-time BDA of individual munitions using unmanned aerial vehicles.

A new concept for generating BDA information relies on a relatively small projectile released from a munition near the target. The dispensed projectile is fitted with a camera so images can be recorded of the target area before and after impact. These images are relayed to suitable receiving platforms such as an airplane which provides real-time BDA information to the battlefield commander. In future fast-paced battlefield environments, units with the ability to obtain accurate real-time BDA information will enjoy a distinct advantage on the battlefield, leading to a more lethal and efficient fighting force.

In an effort to investigate the potential for real-time image generation using a sensor projectile, Costello [1] simulated the motion of a munition connected to a sensor projectile through a flexible tether. The projectiles were modeled using rigid 6 deg of freedom models while the tether was modeled using a sequence of beads. Since the tether tends to equate the speed of both the munition and sensor projectiles, the duration of time that the sensor projectile is able to view the target after impact is small and for the example shown was under 1 s. Very high loads within the tether line were noted at the point when the tether line was fully extended. Later, Frost and Costello [2, 3] showed that tether line loads are significantly reduced with the use of

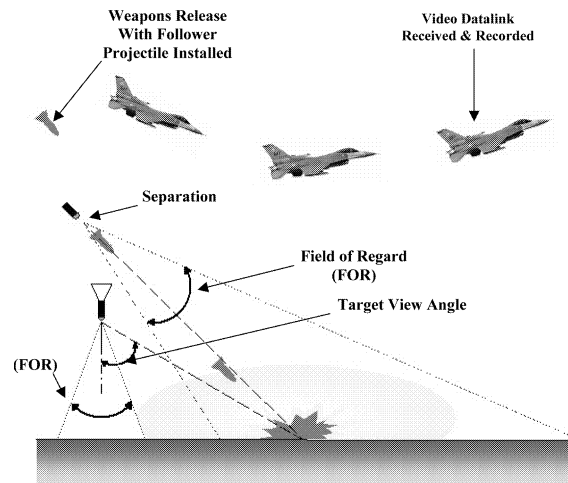


Fig. 1.

friction devices in the tether reel. The work reported here seeks to notably increase the target view time after munition impact beyond what is possible with a tethered system. This is accomplished by removing the tether from the system. Through dynamic simulation, the flight mechanics of a sensor projectile dispensed from a dropped munition are investigated. Parametric studies on the effect of physical system parameters on target view time, separation distance between the sensor projectile and the target, and the maximum acceleration of the sensor projectile are conducted.

MUNITION AND SENSOR PLATFORM DYNAMIC MODEL

The dynamic event considered here consists of a munition that is released from a parent aircraft toward a fixed ground target. In the description to follow, the munition is denoted the lead projectile. The munition contains a relatively small projectile toward the rear of the body. The small projectile is fitted with a camera in the nose with the lens aligned along the projectile axis of symmetry. This projectile is called the follower projectile. The follower projectile is not exposed to external air flow while connected to the lead projectile. At a specific time after the lead projectile is released from the parent aircraft, the follower projectile is ejected from the lead projectile by a force that acts equal and opposite along the bodies' axis of symmetry. Angular rates and crossing velocities caused by asymmetrical pressure are not considered. This time is denoted as the follower projectile separation time t_{ST} . In order to reduce the speed of the follower projectile, a ballute is deployed from the follower projectile shortly after release from the lead projectile. The time between the follower projectile separation time and the time that the ballute is deployed is called the ballute deployment time t_{BD} . The ballute is assumed to inflate instantaneously. A schematic of the overall event is given in Fig. 1.

Each projectile is modeled as a rigid body with 6 deg of freedom. The degrees of freedom for each projectile include three position components of the mass center of the projectile as well as three Euler orientation angles of the body. The equations of motion for either projectile are provided in (1)–(4) [5, 6]

$$\begin{Bmatrix} \dot{x} \\ \dot{y} \\ \dot{z} \end{Bmatrix} = \begin{bmatrix} c_\theta c_\psi & s_\phi s_\theta c_\psi - c_\phi s_\psi & c_\phi s_\theta c_\psi + s_\phi s_\psi \\ c_\theta s_\psi & s_\phi s_\theta s_\psi + c_\phi c_\psi & c_\phi s_\theta s_\psi - s_\phi c_\psi \\ -s_\theta & s_\phi c_\theta & c_\phi c_\theta \end{bmatrix} \begin{Bmatrix} u \\ v \\ w \end{Bmatrix} \quad (1)$$

$$\begin{Bmatrix} \dot{\phi} \\ \dot{\theta} \\ \dot{\psi} \end{Bmatrix} = \begin{bmatrix} 1 & s_\phi t_\theta & c_\phi t_\theta \\ 0 & c_\phi & -s_\phi \\ 0 & s_\phi/c_\theta & c_\phi/c_\theta \end{bmatrix} \begin{Bmatrix} p \\ q \\ r \end{Bmatrix} \quad (2)$$

$$\begin{Bmatrix} \dot{u} \\ \dot{v} \\ \dot{w} \end{Bmatrix} = \begin{Bmatrix} X/m \\ Y/m \\ Z/m \end{Bmatrix} - \begin{bmatrix} 0 & -r & q \\ r & 0 & -p \\ -q & p & 0 \end{bmatrix} \begin{Bmatrix} u \\ v \\ w \end{Bmatrix} \quad (3)$$

$$\begin{Bmatrix} \dot{p} \\ \dot{q} \\ \dot{r} \end{Bmatrix} = [I]^{-1} \left[\begin{Bmatrix} L \\ M \\ N \end{Bmatrix} - \begin{bmatrix} 0 & -r & q \\ r & 0 & -p \\ -q & p & 0 \end{bmatrix} [I] \begin{Bmatrix} p \\ q \\ r \end{Bmatrix} \right]. \quad (4)$$

Both projectiles have applied load contributions from weight (W), body aerodynamic forces (A), and separation forces (S). The follower projectile also has additional applied forces due to ballute aerodynamic forces (B)

$$\begin{Bmatrix} X \\ Y \\ Z \end{Bmatrix} = \begin{Bmatrix} X_W \\ Y_W \\ Z_W \end{Bmatrix} + \begin{Bmatrix} X_A \\ Y_A \\ Z_A \end{Bmatrix} + \begin{Bmatrix} X_S \\ Y_S \\ Z_S \end{Bmatrix} + \begin{Bmatrix} X_B \\ Y_B \\ Z_B \end{Bmatrix}. \quad (5)$$

The projectile weight contribution is given by (6),

$$\begin{Bmatrix} X_W \\ Y_W \\ Z_W \end{Bmatrix} = mg \begin{Bmatrix} -s_\theta \\ s_\phi c_\theta \\ c_\phi c_\theta \end{Bmatrix} \quad (6)$$

while the body aerodynamic force contribution, which acts at the center of pressure of the projectile, is given by (7)

$$\begin{Bmatrix} X_A \\ Y_A \\ Z_A \end{Bmatrix} = -\frac{\pi}{8} \rho V^2 D^2 \begin{Bmatrix} C_{X0} + C_{X2}(v^2 + w^2)/V^2 \\ C_{NA}v/V \\ C_{NA}w/V \end{Bmatrix}. \quad (7)$$

To separate the projectiles, an equal and opposite force acting over a short time interval is exerted on both bodies. Equation (8) provides an expression for the separation force during projectile separation

$$\begin{Bmatrix} X_S \\ Y_S \\ Z_S \end{Bmatrix} = aF_S \begin{Bmatrix} n_X \\ n_Y \\ n_Z \end{Bmatrix}. \quad (8)$$

When the two projectiles are not separating, the separation force is zero. For the lead projectile $a = 1$ while for the follower projectile $a = -1$. The ballute aerodynamic force is modeled as a parachute with drag

$$\begin{Bmatrix} X_B \\ Y_B \\ Z_B \end{Bmatrix} = -\frac{1}{8} \rho V \pi D_B^2 C_D \begin{Bmatrix} u \\ v \\ w \end{Bmatrix}. \quad (9)$$

The applied moments about the projectile mass center contains contributions from the steady air load (SA), unsteady air load (UA), separation force (S), and ballute aerodynamic force (B)

$$\begin{Bmatrix} L \\ M \\ N \end{Bmatrix} = \begin{Bmatrix} L_{SA} \\ M_{SA} \\ N_{SA} \end{Bmatrix} + \begin{Bmatrix} L_{UA} \\ M_{UA} \\ N_{UA} \end{Bmatrix} + \begin{Bmatrix} L_S \\ M_S \\ N_S \end{Bmatrix} + \begin{Bmatrix} L_B \\ M_B \\ N_B \end{Bmatrix}. \quad (10)$$

The moment components due to the steady aerodynamic force, separation force, and ballute aerodynamic force are computed with a cross product between the distance vector from the mass center of the projectile to the location of the specific force and the force itself. The unsteady body aerodynamic moment provides a damping source for projectile angular motion and is given by (11)

$$\begin{Bmatrix} L_{UA} \\ M_{UA} \\ N_{UA} \end{Bmatrix} = \frac{\pi}{8} \rho V^2 D^3 \begin{Bmatrix} C_{DD} + \frac{pDC_{LP}}{2V} \\ \frac{qDC_{MQ}}{2V} \\ \frac{rDC_{MQ}}{2V} \end{Bmatrix}. \quad (11)$$

The center of pressure location and all aerodynamic coefficients depend on local Mach number.

During the initial phase of flight when the lead and follower projectiles are rigidly connected, the mass, mass center location, and inertial properties of the lead projectile are based on the composite body. During this stage of the simulation, the motion of the follower projectile is generated from kinematic relationships. At separation, the lead projectile mass and inertia properties are updated to reflect the loss of the follower projectile from the body.

SYSTEM PERFORMANCE METRICS

Proper design of a real-time BDA system requires the follower projectile to record images of the target area after lead projectile impact. In order for the follower projectile to record useful images for BDA analysis, the target must be within the field of regard (FOR) of the follower projectile camera. Furthermore, the follower projectile must be within a prescribed distance of the target so that the lead projectile and target effects are visible on the recorded images. Moreover, since the follower projectile

contains sensitive components, the follower projectile maximum acceleration must be limited. The FOR is defined as 2 times the angle between the axis and the side of a cone aligned along the projectile axis of symmetry.

The design requirements stated above can be encapsulated into three performance parameters of the BDA system, namely, the view time Γ_{VT} , the separation distance Γ_{SD} , and the maximum acceleration of the follower projectile Γ_{MA} . The view time is defined as the total duration of time that the target remains within the FOR of the follower projectile camera after impact of the lead projectile. BDA analysts seek to maximize the view time in order to maximize raw BDA data. To compute the view time, first note that the distance vector from the follower projectile to the target expressed in the follower projectile reference frame is given by (12)

$$\begin{pmatrix} e_X \\ e_Y \\ e_Z \end{pmatrix} = \begin{bmatrix} c_{\theta_F} c_{\psi_F} & c_{\theta_F} s_{\psi_F} & -s_{\theta_F} \\ s_{\phi_F} s_{\theta_F} c_{\psi_F} - c_{\phi_F} s_{\psi_F} & s_{\phi_F} s_{\theta_F} s_{\psi_F} + c_{\phi_F} c_{\psi_F} & s_{\phi_F} c_{\theta_F} \\ c_{\phi_F} s_{\theta_F} c_{\psi_F} + s_{\phi_F} s_{\psi_F} & c_{\phi_F} s_{\theta_F} s_{\psi_F} - s_{\phi_F} c_{\psi_F} & c_{\phi_F} c_{\theta} \end{bmatrix} \times \begin{pmatrix} x_T - x_F \\ y_T - y_F \\ z_T - z_F \end{pmatrix}. \quad (12)$$

The angle between the follower projectile centerline and the target $\gamma_{FOV}/2$, is known as the target view angle and is computed with (13),

$$\gamma_{FOV} = 2 \tan^{-1} \left(\sqrt{e_Y^2 + e_Z^2} / e_X \right) \quad (13)$$

while the follower projectile camera FOR is denoted δ_{FOR} . The target is within the FOR of the camera if $\gamma_{FOV} \leq \delta_{FOR}$. Using (12), the separation distance is defined as the total distance between the follower projectile and the target at the instant when the lead projectile impacts the ground

$$\Gamma_{SD} = \sqrt{e_{X_I}^2 + e_{Y_I}^2 + e_{Z_I}^2}. \quad (14)$$

In (14), the subscript I indicates values of e_X , e_Y , e_Z at the time of lead projectile impact. The body frame components of the acceleration of the mass center of the follower projectile are given in (15)

$$\begin{pmatrix} a_X \\ a_Y \\ a_Z \end{pmatrix} = \begin{pmatrix} \dot{u} \\ \dot{v} \\ \dot{w} \end{pmatrix} + \begin{bmatrix} 0 & -r & q \\ r & 0 & -p \\ -q & p & 0 \end{bmatrix} \begin{pmatrix} u \\ v \\ w \end{pmatrix} + \begin{bmatrix} -q^2 - r^2 & pq - \dot{r} & pr + \dot{q} \\ pq + \dot{r} & p^2 - r^2 & qr - \dot{p} \\ pr - \dot{q} & qr + \dot{p} & p^2 - q^2 \end{bmatrix} \begin{pmatrix} SL_C - SL_{CG} \\ BL_C - BL_{CG} \\ WL_C - WL_{CG} \end{pmatrix}. \quad (15)$$

For a given trajectory, the maximum of the magnitude of the mass center acceleration for the follower

projectile is given by (16)

$$\Gamma_{MA} = \max \left(\sqrt{a_X^2 + a_Y^2 + a_Z^2} \right). \quad (16)$$

Generally, Γ_{MA} occurs either when the follower projectile is released from the lead projectile or when the ballute is deployed from the follower projectile.

RESULTS

The equations of motion described above are numerically integrated using a fourth-order Runge-Kutta algorithm to generate the trajectory of both the lead and follower projectiles from the point of release from the parent aircraft to impact of the follower projectile with the ground. Simulations under different conditions are performed so that the dynamic performance of this real-time BDA system can be evaluated. The lead projectile used in the simulation study that follows is a standard 2000 lbf bomb. The bomb is a 9 ft long, fin stabilized projectile with four fins mounted on the tail. Initially, the follower projectile is rigidly attached to the lead projectile. The lead projectile mass center location from the base, the roll inertia, and the pitch inertia after the sensor projectile is dispensed are 7.4 ft, 19.7 slug ft², and 405 slug ft², respectively. Aerodynamic coefficient data for the lead projectile were obtained from a range test reported by Wong, Whyte, and Gates [7]. The follower projectile is a 1 ft long, 5 lbf fin stabilized projectile. The mass center with respect to the base of the projectile, the roll inertia, and the pitch inertia are 0.5 ft, 0.0015 slug ft², and 0.01 slug ft², respectively. Aerodynamic coefficient input data for the sensor projectile was predicted using the projectile design and analysis computer code PRODAS [8]. A 12 in diameter ballute is deployed from the follower projectile. The simulation results do not include atmospheric winds.

For the baseline simulation shown in Figs. 2–9, the lead projectile is released from a parent aircraft flying straight and level at a speed of 500 kt and an altitude of 30,000 ft. The follower projectile is released from the lead projectile at an altitude of approximately 5000 ft which occurs 41.5 s after munition release from the parent aircraft. Fig. 2 plots altitude versus range of the projectiles which shows that the projectiles travel 35,000 ft down range as they drop from an altitude of 30,000 ft in approximately 45 s. Follower projectile range is less than the lead projectile due to the fact that the follower projectile has a higher drag coefficient and lower weight. The follower projectile remains aloft approximately 9 s longer than the lead projectile. Pitch angle of both projectiles is shown in Fig. 3. The lead projectile pitches down throughout the trajectory from an initial level pitch attitude to slightly greater than 60 deg nose down at impact. The follower

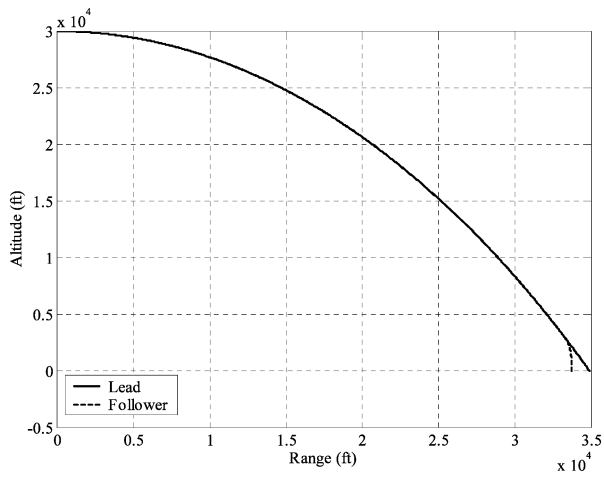


Fig. 2. Altitude versus range (drop altitude = 30,000 ft, drop velocity = 500 kt, solid = lead projectile, dashed = follower projectile).

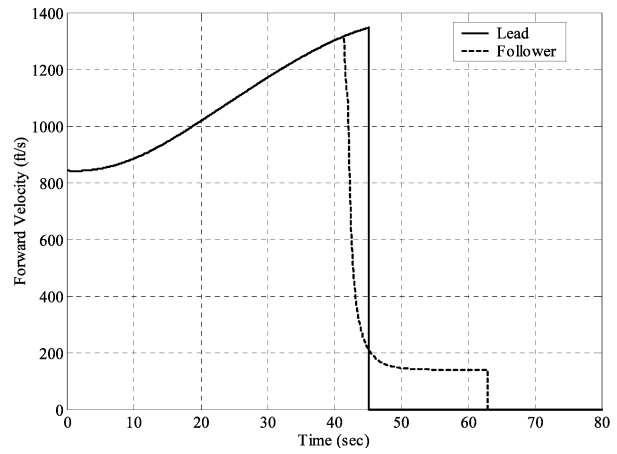


Fig. 4. Forward body velocity component versus time (drop altitude = 30,000 ft, drop velocity = 500 kt, solid=lead projectile, dashed = follower projectile).

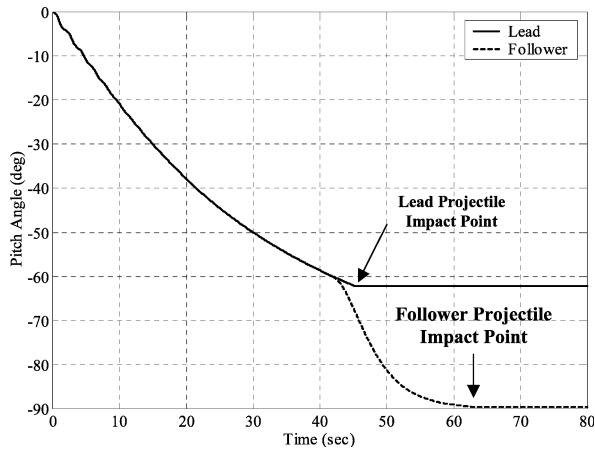


Fig. 3. Euler pitch angle versus time (drop altitude = 30,000 ft, drop velocity = 500 kt, solid = lead projectile, dashed = follower projectile).

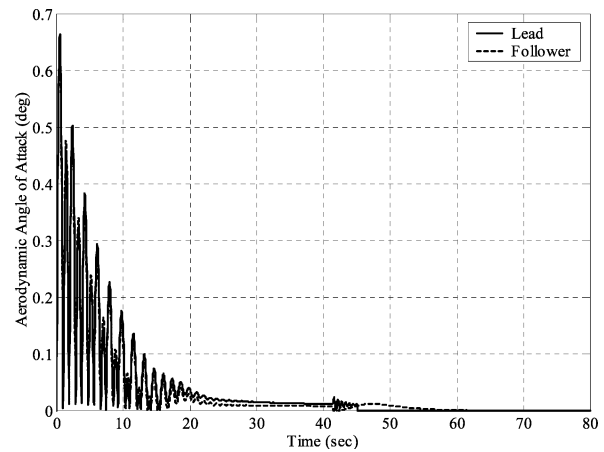


Fig. 5. Aerodynamic angle of attack versus time (drop altitude = 30,000 ft, drop velocity = 500 kt, solid = lead projectile, dashed = follower projectile).

projectile is released from the lead projectile with a pitch attitude of approximately 60 nose down and it continues to pitch nose down through its trajectory. When the follower projectile impacts the ground, it is essentially pointed directly toward the ground. The forward body velocity time responses are shown in Fig. 4. Because the lead projectile is released at a speed which is less than its steady state drop velocity, its speed increases as it falls toward the ground until it impacts the ground surface 45 s into flight. Conversely, the follower projectile is released from the lead projectile at a speed that is greater than its steady state drop velocity so its speed is reduced after being released from the lead projectile from an initial speed of 1,350 ft/s to 150 ft/s at impact. Both off-axis velocity components for the lead and follower projectiles remain relatively small over the duration of the trajectory indicating that their aerodynamic angles of attack also remain small as shown in Figs. 5. The frequency of vibration is notably smaller for the lead

projectile compared with the follower projectile as the follower projectile mass and inertia are smaller, leading to higher frequency angle of attack vibration. Prior to separation a kinematic relationship is used to determine the behavior of the follower projectile. The follower projectile does not lie on the center of gravity of the lead projectile; therefore the angles of attack of the two bodies before separation do not correspond exactly. Fig. 6 displays the follower projectile mass center acceleration. Two spikes are shown which correspond to separation of the follower projectile from the lead projectile and deployment of the ballute on the follower projectile. While this is not the case shown in Fig. 6, the largest acceleration occurs when the ballute is deployed at the same time the follower projectile is released from the lead projectile. Fig. 7 plots the separation distance between the follower projectile and the target. At the time when the lead projectile impacts the ground, the follower projectile is 3000 ft from the target. When the follower projectile impacts the ground, the separation distance is 1200 ft

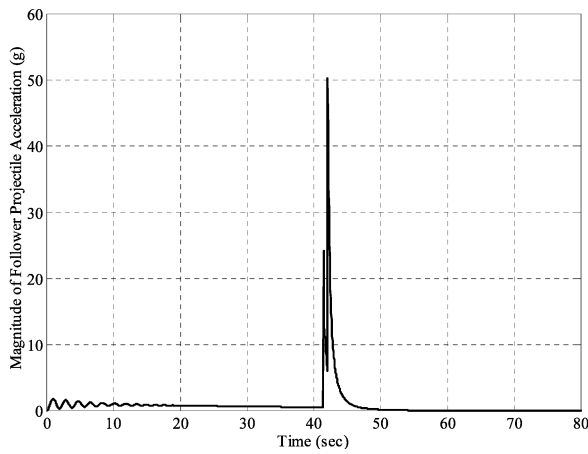


Fig. 6. Magnitude of follower projectile acceleration versus time (drop altitude = 30,000 ft, drop velocity = 500 kt).

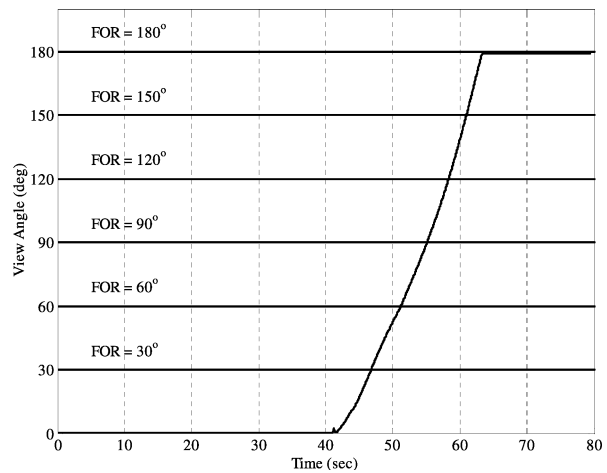


Fig. 8. View angle versus time (drop altitude = 30,000 ft, drop velocity = 500 kt).

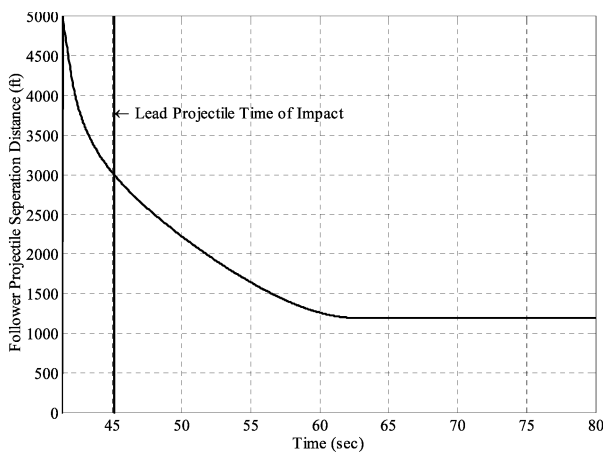


Fig. 7. Follower projectile separation distance versus time (drop altitude = 30,000 ft, drop velocity = 500 kt).

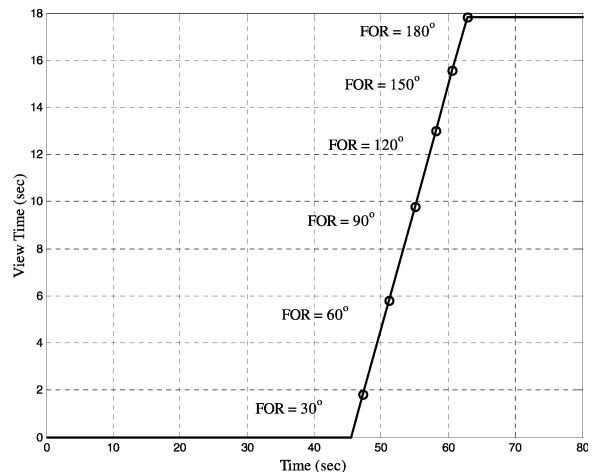


Fig. 9. Accumulated view time versus time (drop altitude = 30,000 ft, drop velocity = 500 kt).

due to the fact that the follower projectile range is less than the lead projectile. In Fig. 8, the target view angle is contrasted against different camera FOR values. As the FOR of the follower projectile camera is increased, the view time increases. Notice that the view angle steadily increases, indicating that the target steadily moves away from the center of the camera until it finally is out of the camera FOR. Fig. 9 presents the accumulated view time over the trajectory for different camera FOR. As the FOR of the follower projectile camera is increased, the view time continues to increase, as expected, but at a decreasing rate suggesting a diminishing return of view time for increased camera FOR.

In order to understand how the fundamental performance metrics of the BDA system are interrelated, a matrix of different combinations of follower projectile separation time and ballute deployment time are evaluated. Fig. 10 shows how the maximum of the mass center acceleration of the sensor projectile varies as a function of the follower projectile separation time and ballute deployment

time. For a given follower projectile separation time, the maximum follower projectile acceleration is when the ballute deployment time is zero. The maximum acceleration rapidly decreases as ballute deployment time increases as can be seen by the large discontinuity at a ballute separation delay of approximately 0.1 s. It can be seen from Fig. 5 that there are two separate acceleration peaks for the follower projectile. The first one is due to the release from the lead and the second one is due to the ballute deployment. The closer these peaks coincide the greater the magnitude of the acceleration is amplified. Once the ballute deployment delay becomes large enough that the peaks no longer coincide the magnitude of the acceleration is only due to the greater of the two peaks and not a combination of both of them. Furthermore, for a given ballute deployment time, the maximum follower projectile acceleration increases with increased follower projectile separation time due to the fact that the

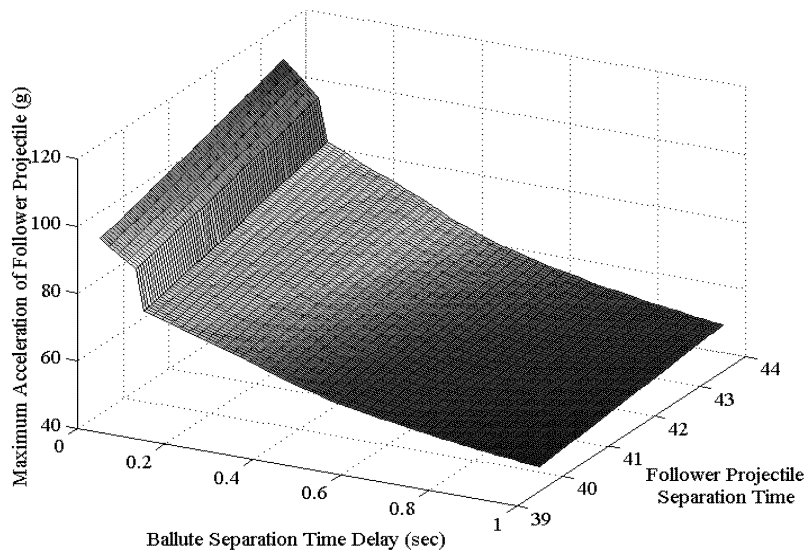


Fig. 10. Follower projectile maximum acceleration versus follower projectile separation time and ballute separation time (drop altitude = 30,000 ft, drop velocity = 500 kt).

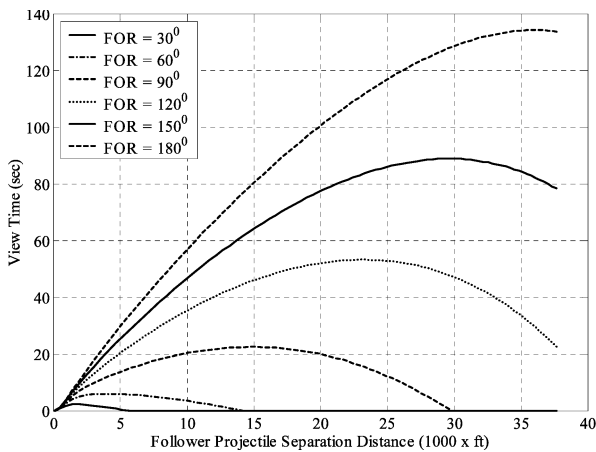


Fig. 11. View time versus separation distance (drop altitude = 30,000 ft, drop velocity = 500 kt).

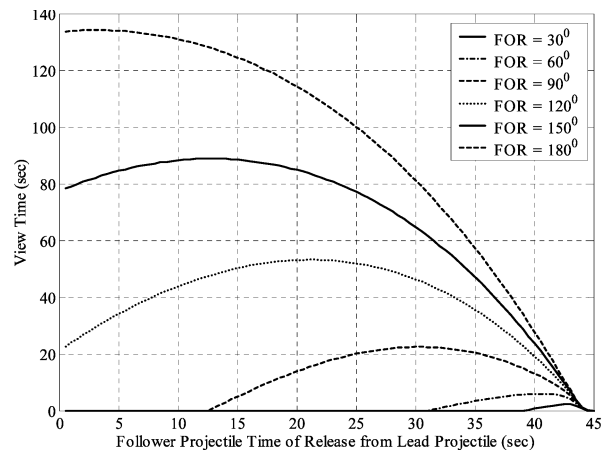
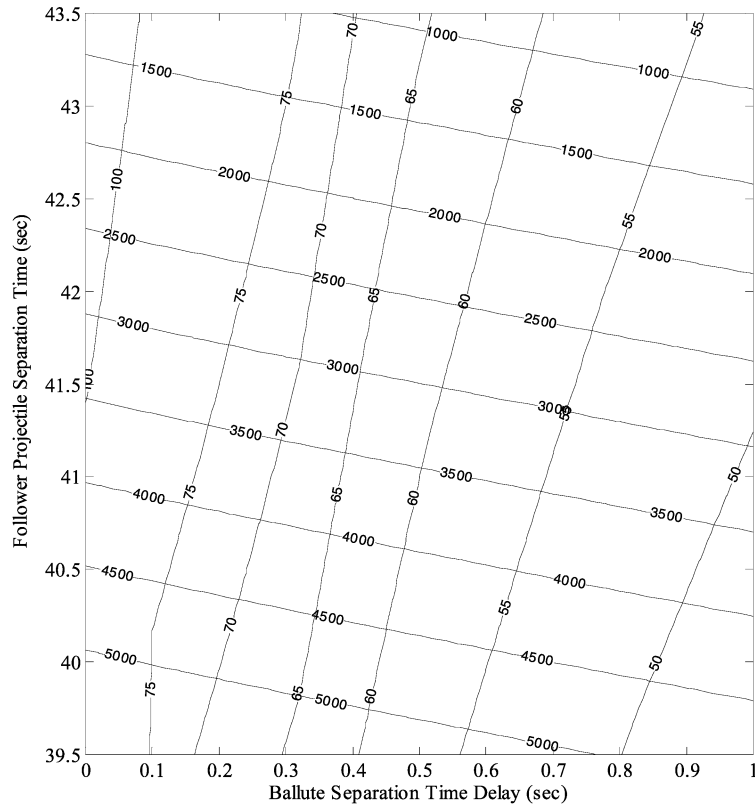


Fig. 12. View time versus release time (drop altitude = 30,000 ft, drop velocity = 500 kt).

follower projectile speed at release is greater. For a matrix of different follower projectile separation times and ballute deployment times, view time and separation distance were obtained for different camera FOR values. The results are plotted in Fig. 11. The follower projectile separation times and ballute deployment times dictate the amount of separation distance, and consequently the amount of view time achieved. A unique relationship between view time and separation distance is noticed for a given camera FOR. Furthermore, for a given camera FOR a unique maximum view time exists. At points other than the maximum view time point, a given view time can be attained at two different separation distances. As the camera FOR is increased, the view time is increased and the maximum view time point moves out to higher values of separation distance. Fig. 11 also shows that for a given separation distance, different view times can be attained depending

on the camera FOR. Fig. 12 shows the effect of follower projectile release time on target view time. As expected, maximum view time increases as camera FOR increases. However, for small camera FOR and low values for follower projectile release time, the target moves out of the camera FOR before lead projectile impact hence the view time is zero. The follower projectile release time for maximum target view time increases as camera FOR decreases. Fig. 13 presents a BDA system performance plot that relates maximum acceleration of the follower projectile, view time, and separation distance. The vertical contour lines represent lines of constant maximum follower projectile acceleration whereas the horizontal contour lines represent lines of constant separation distance. As ballute separation time is increased and follower projectile separation time is decreased, follower projectile maximum acceleration is decreased. Also, as ballute separation time is



Separation Distance Lines	1000 feet	1500 feet	2000 feet	2500 feet	3000 feet	3500 feet	4000 feet	4500 feet	5000 feet
View Time for a FOR = 30 degrees	1.95	2.32	2.3	2.11	1.85	1.56	1.24	0.89	0.52
View Time for a FOR = 60 degrees	3.08	4.38	5.17	5.62	5.87	6	6.07	6.08	6.02
View Time for a FOR = 90 degrees	3.69	5.76	7.4	8.75	9.91	10.98	11.98	12.94	13.83
View Time for a FOR = 120 degrees	4.08	6.74	9.05	11.14	13.09	14.97	16.81	18.61	20.35
View Time for a FOR = 150 degrees	4.33	7.43	10.37	13.15	15.77	18.24	20.56	22.71	24.88
View Time for a FOR = 180 degrees	4.43	7.94	11.34	14.64	17.82	20.89	23.86	24.88	24.88

Fig. 13. BDA system performance diagram (drop altitude = 30,000 ft, drop velocity = 500 kt).
 Vertical contour lines = constant maximum follower projectile acceleration (gs).
 Horizontal contour lines = constant follower projectile separation distance (ft).

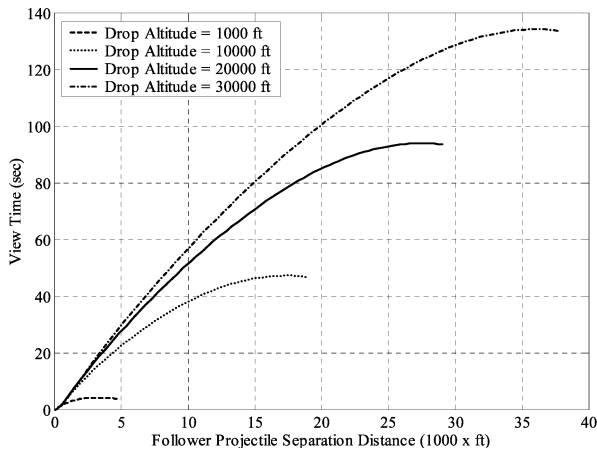


Fig. 14. View time versus separation distance (drop velocity = 500 kt, FOR = 180°).

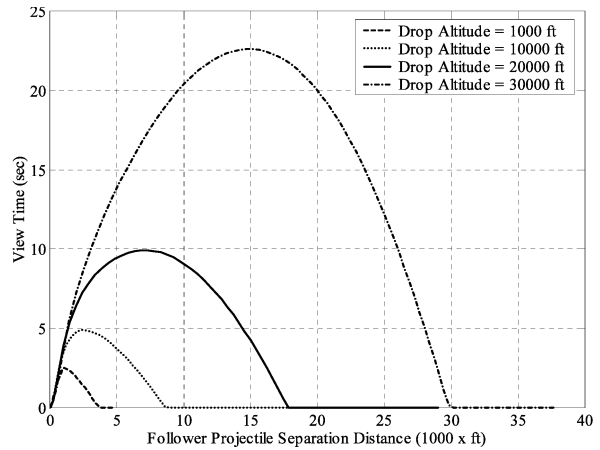


Fig. 15. View time versus separation distance (drop velocity = 500 kt, FOR = 90°).

increased and follower projectile separation time is increased, separation distance is decreased. For a given separation distance, the table at the bottom of the chart can be used to determine the view time

for a given camera FOR angle. For example, for an impact separation distance equal to 3000 ft, a view time of 9.91 s, and a maximum follower projectile acceleration of 55gs, the required follower projectile

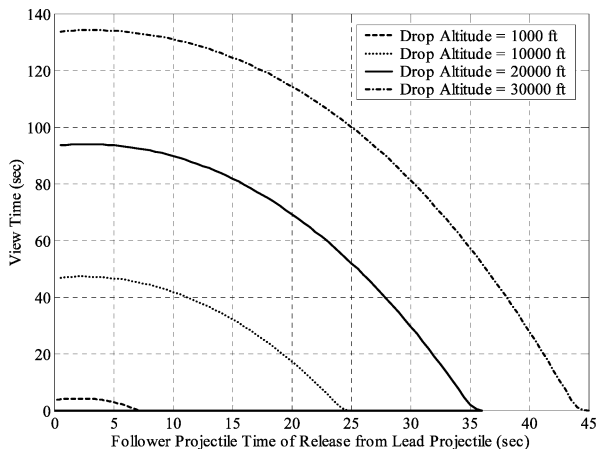


Fig. 16. View time versus release time (drop velocity = 500 kt, FOR = 180°).

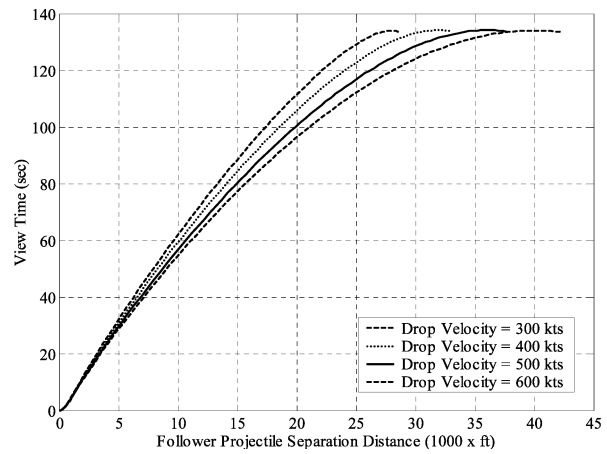


Fig. 18. View time versus separation distance (drop altitude = 30,000 ft, FOR = 180°).

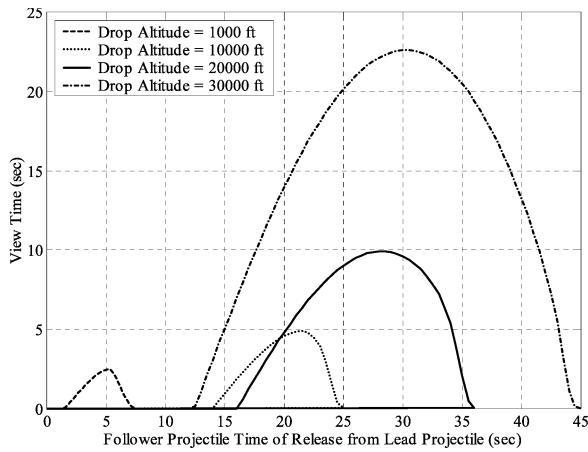


Fig. 17. View time versus release time (drop velocity = 500 kt, FOR = 90°).

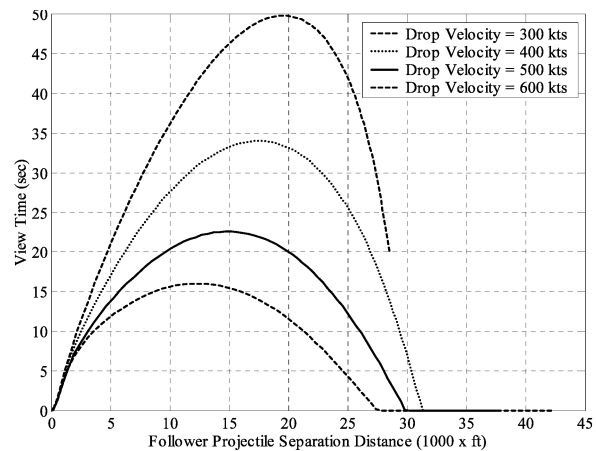


Fig. 19. View time versus separation distance (drop altitude = 30,000 ft, FOR = 90°).

separation time is 41.35 s, the ballute deployment is 0.72 s, and the required camera FOR is 90 deg. This system performance plot provides a convenient design tool to display key interactions between fundamental design parameters.

The baseline simulation results shown in Figs. 2–13 consider a 30,000 ft munition release altitude. Figs. 14–17 explore the effect of munition drop altitude on target view time and separation distance for camera FOR of 180 deg and 90 deg. Generally, as drop altitude is increased, view time is also increased. In the case of a large camera FOR of 180 deg, the target remains within the camera FOR until it impacts the ground and view time is limited by the time the follower projectile remains aloft. In the case of a relatively small camera FOR of 90 deg, target view time is limited due to the target exiting the camera FOR before the follower projectile impacts the ground. For a large camera FOR, maximum view time is attained by releasing the follower projectile at the same time that the munition is released from the parent aircraft. However, for a small camera FOR of 90 deg, maximum target view time is realized at a unique follower projectile release time that tends

to increase as the munition drop altitude increases. This is due to the fact that if the camera is released too early, the target will exit the camera FOR before the follower projectile impacts the ground.

The baseline simulation results shown in Figs. 2–13 consider a 500 kt munition release speed. Figs. 18–21 explore the effect of munition drop speed on target view time and separation distance for camera FOR of 180 deg and 90 deg. Generally, as drop speed is increased, view time is decreased. For a large camera FOR of 180 deg, view time and separation distance are altered slightly whereas for a small camera FOR of 90 deg, drop velocity significantly alters view time and separation distance characteristics. For a large camera FOR, the release time essentially dictates the view time regardless of the drop velocity. However, for a smaller camera FOR of 90 deg, view time is highly dependent on the munition drop velocity.

Figs. 22 and 23 show how system performance changes with follower projectile weight and drag coefficient. As shown in Fig. 22, for a given follower projectile weight, view time increases as camera FOR

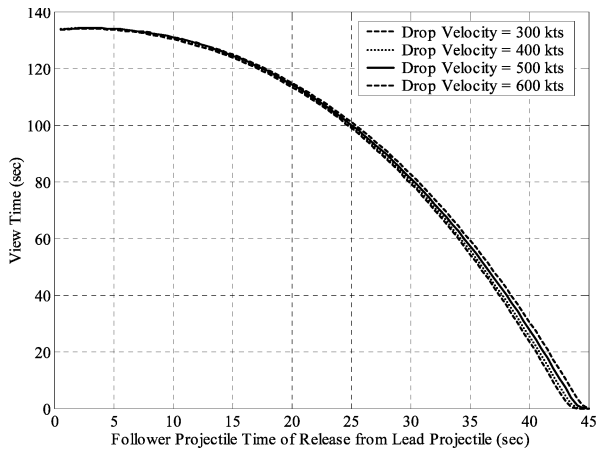


Fig. 20. View time versus release time (drop altitude = 30,000 ft, FOR = 180°).

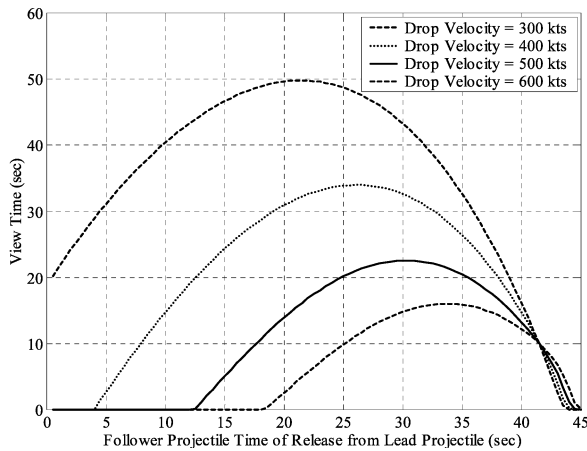


Fig. 21. View time versus release time (drop altitude = 30,000 ft, FOR = 90°).

is increased. As the camera FOR increases, the rate of increase of view time is reduced. As the weight of the follower projectile is increased, the separation distance after lead projectile impact is reduced since the follower projectile falls toward the ground more rapidly. Furthermore, reduced follower projectile weight yields greater view time since the follower projectile remains aloft longer. As shown in Fig. 23, higher values of follower projectile drag coefficient provide for larger separation distance after lead projectile impact since follower projectile speed is reduced by a greater drag force. Also, larger values of follower projectile drag coefficient yield larger values of view time. However, larger values of follower projectile drag coefficient also yield higher maximum acceleration of the follower projectile.

CONCLUSIONS

A camera projectile released from a munition can obtain useful BDA images. A fundamental compromise between the duration of time that a target can be viewed after munition impact and the separation distance between the follower projectile and

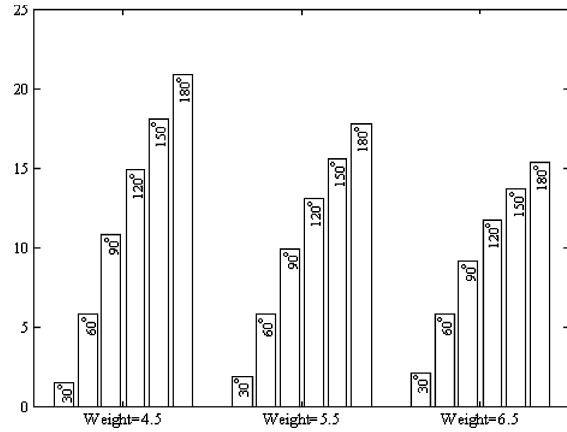


Fig. 22. View time versus camera for and follower projectile weight (drop altitude = 30,000 ft, drop velocity = 500 kt).

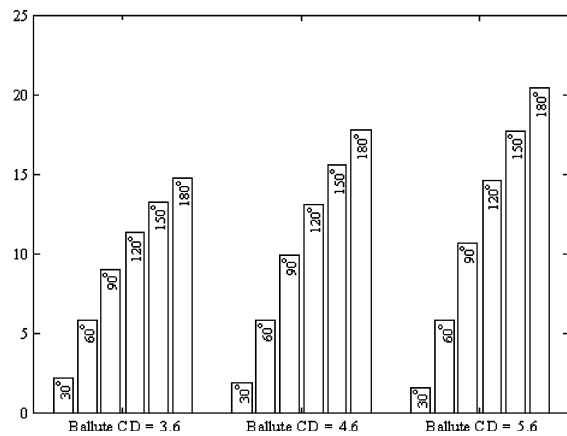


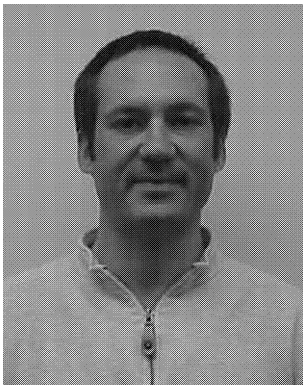
Fig. 23. View time versus camera for and ballute drag coefficient (drop altitude = 30,000 ft, drop velocity = 500 kt).

the target at impacts exists. Longer view times dictate larger separation distances at impact. A ballute that is deployed from the follower projectile can significantly increase system performance, in terms of view time, by increasing the drag force on the body and decreasing the drop velocity of the follower projectile. However, to minimize the acceleration of the follower projectile, ballute deployment from the follower projectile should be delayed slightly. The relationships between the basic system design parameters, namely, view time, separation distance, and maximum follow projectile acceleration can be conveniently displayed on a single system performance diagram. As munition release altitude is increased or munition release speed is decreased, view time is increased.

REFERENCES

- [1] Costello, M. (1999) Simulation of two projectiles connected by a flexible tether for bomb damage assessment. Technical Report, Air Force Research Laboratory, Air Force Material Command, Eglin Air Force Base, AFRL-MN-EG-TR-1999-7003, 1999.

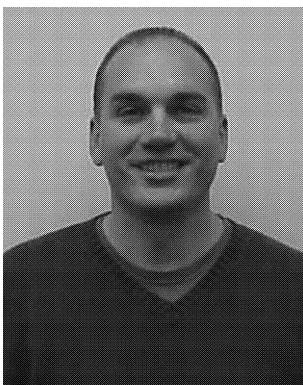
- [2] Frost, G., and Costello, M. (2000)
Two projectiles connected by a flexible tether dropped in the atmosphere.
Journal of Guidance, Control, and Dynamics, **23**, 6 (2000).
- [3] Frost, G., and Costello, M. (2000)
Improved deployment characteristics of a tether connected munition system.
Journal of Guidance, Control, and Dynamics, **24**, 3 (2001).
- [4] Gast, R., Morris, S., and Costello, M. (2000)
Simulation of shot impacts for the M1A1 tank gun.
Journal of Guidance, Control, and Dynamics, **23**, 1 (2000), 53–59.
- [5] Costello, M., and Anderson, D. (1996)
Effect of internal mass unbalance on the terminal accuracy and stability of a projectile.
In *Proceedings of the 1996 AIAA Flight Mechanics Conference*, San Diego, CA, 1996.
- [6] Wong, B. C., Whyte, R. H., and Gates, R. S. (1986)
Aerodynamic comparison of the Mark 84 and improved 2000-pound bomb configurations.
Technical Report, Air Force Armament Laboratory, AFATL-TR-85-38, Jan. 1986.
- [7] Whyte, R., and Hathaway, W. (2003)
PRODAS—Projectile Design and Analysis Computer Aided Engineering Tool.
Arrowtech Associates, Burlington, VT, 2003.



Geoffrey Frost received a B.S. degree from the University of Tennessee, Knoxville, in 1991, and an M.S. degree from Oregon State University, Corvallis, in 1999, both in mechanical engineering.

He worked for several years as an engineer for Kimberly Clark, Inc. He is currently a Ph.D. candidate in the Department of Mechanical Engineering at Oregon State University. His area of specialization is dynamic systems, measurement, and control.

Mr. Frost is a recipient of an ORISE Fellowship from the U.S. Army.



Mark Costello received a B.S. degree from The Pennsylvania State University, in 1987, and the M.S. and Ph.D. degrees from the Georgia Institute of Technology, in 1989 and 1992, respectively, all in aerospace engineering.

He was on the faculty at the U.S. Military Academy in the Department of Civil and Mechanical Engineering from 1993 to 1998. He is currently an assistant professor in the Department of Mechanical Engineering at Oregon State University. His teaching and research interests lie at the intersection of dynamic modeling and analysis, control, and design of mechanical and aeronautical systems.